Journal of Neuroscience Research 54:734–753 (1998)

Hippocampal AMPA and NMDA mRNA Levels Correlate With Aberrant Fascia Dentata Mossy Fiber Sprouting in the Pilocarpine Model of Spontaneous Limbic Epilepsy

Gary W. Mathern,[1,4,5]* **James K. Pretorius,**[5] **Delia Mendoza,**[5] **Alana Lozada,**[5] **and Harley I. Kornblum**[2,3,5]

[1]Division of Neurosurgery, University of California-Los Angeles, Los Angeles, California
[2]Department of Pediatrics, University of California-Los Angeles, Los Angeles, California
[3]Department of Molecular and Medical Pharmacology, University of California-Los Angeles, Los Angeles, California
[4]Mental Retardation Research Center, University of California-Los Angeles, Los Angeles, California
[5]The Brain Research Institute, University of California-Los Angeles, Los Angeles, California

There is considerable controversy whether aberrant fascia dentata (FD) mossy fiber sprouting is an epiphenomena related to neuronal loss or a pathologic abnormality responsible for spontaneous limbic seizures. If mossy fiber sprouting contributes to seizures, then reorganized axon circuits should alter postsynaptic glutamate receptor properties. In the pilocarpine-status rat model, this study determined if changes in alpha amino-3-hydroxy-5-methyl-4-isoxazole-propionate (AMPA) and n-methyl-D-aspartic acid (NMDA) receptor subunit mRNA levels correlated with mossy fiber sprouting. Sprague-Dawley rats were injected with pilocarpine (320 mg/kg; i.p.) and maintained in status epilepticus for 6 to 8 hours (pilocarpine-status). Rats were killed during the: (1) latent phase after neuronal loss but before spontaneous limbic seizures (day 11 poststatus; n = 7); (2) early seizure phase after their first seizures (day 25; n = 7); and (3) chronic seizure phase after many seizures (day 85; n = 9). Hippocampi were studied for neuron counts, inner molecular layer (IML) neo-Timm's staining, and GluR1–3 and NMDAR1–2b mRNA levels. Compared with controls, pilocarpine-status rats in the: (1) latent phase showed increased FD GluR3, NMDAR1, and NMDAR2b; greater CA4 and CA1 NMDAR1; and decreased subiculum GluR1 hybridization densities; (2) early seizure phase showed increased FD GluR3, increased CA1 NMDAR1, and decreased subiculum NMDAR2b densities; and (3) chronic seizure phase showed increased FD GluR2; increased FD and CA4 GluR3; decreased CA1 GluR2; and decreased subiculum GluR1, GluR2, NMDAR1, and NMDAR2b levels. In multivariate analyses, greater IML neo-Timm's staining: (1) positively correlated with FD GluR3 and NMDAR1 and (2) negatively correlated with CA1 and subiculum GluR1 and GluR2 mRNA levels. These results indicate that: (1) hippocampal AMPA and NMDA receptor subunit mRNA levels changed as rats progressed from the latent to chronic seizure phase and (2) certain subunit alterations correlated with mossy fiber sprouting. Our findings support the hypothesis that aberrant axon circuitry alters postsynaptic hippocampal glutamate receptor subunit stoichiometry; this may contribute to limbic epileptogenesis. J. Neurosci. Res. 54:734–753, 1998.

Key words: glutamate neurotransmission; ionotropic receptors; synaptic reorganization; reactive synaptogenesis; temporal lobe seizures

INTRODUCTION

For more than a decade, there has been vigorous debate whether damage-induced reactive synaptogenesis causes neuronal hyperexcitability and spontaneous seizures. Most of this controversy has centered on the hippocampus and the pathophysiologic relationship between supragranular mossy fiber sprouting and limbic seizures (McNamara, 1994; Dudek and Spitz, 1997).

Contract grant sponsor: NIH; Contract grant numbers: K08 NS 01603, PO1 NS 02808, PO1 NS 28383, NS 28383.

*Correspondence to: Gary W. Mathern, MD, Division of Neurosurgery, Reed Neurological Research Center, UCLA Medical Center, Los Angeles, CA 90095-1769. E-mail: gmathern@ucla.edu

Received 27 August 1998; Revised 10 September 1998; Accepted 14 September 1998

Tauck and Nadler (1985) were the first to show electrophysiologic evidence that mossy fiber sprouting was associated with granule cell hyperexcitability as measured by paired-pulse potentiation. Since then, numerous experimental studies have reported in vitro and in vivo evidence that injury-induced aberrant mossy fiber sprouting is associated with granule cell hyperexcitability and spontaneous limbic seizures (Cronin and Dudek, 1988; Cronin et al., 1992; Mathern et al., 1993, 1997a; Leite et al., 1996; Wuarin and Dudek, 1996). In the hippocampus, these findings support the hypothesis that sprouted axon collaterals result in abnormal axon circuitry leading to seizures (for review, see Dudek et al., 1994; Mathern et al., 1997c; Mathern, 1998a, b). This hypothesis has important clinical relevance in that human hippocampi from temporal lobe epilepsy patients show mossy fiber sprouting and granule cell hyperexcitability similar to experimental studies (de Lanerole et al., 1989; Masukawa et al., 1989; Houser et al., 1990; Isokawa and Levesque, 1991; Babb et al., 1991; Franck et al., 1995; Mathern et al., 1995c). The concept that axon sprouting contributes or causes limbic epilepsy is not without its critiques. Following reactive seizures or status epilepticus, rodent studies have reported decreased gamma-aminobutyric acid (GABA)-mediated inhibition that partially or completely recovers by the time animals display significant mossy fiber sprouting and spontaneous limbic seizures (Franck and Schwartzkroin, 1985; Ashwood et al., 1986; Meier et al., 1992; Mangan et al., 1995). Such results have suggested an alternate hypothesis whereby axon sprouting restores GABAergic function and is adaptive rather than maladaptive. In other words, axon sprouting may not be an abnormal phenomena leading to seizure generation (Sloviter, 1992; Longo and Mello, 1997).

If fascia dentata mossy fiber sprouting is maladaptive and responsible for limbic seizures, then the abnormal axon connections should be associated with changes in excitatory postsynaptic receptor properties. In addition, since reactive synaptogenesis requires many weeks to months to complete, alterations in postsynaptic glutamate receptors as a consequence of mossy fiber sprouting should change in a progressive and prolonged time-dependent manner (Nadler et al., 1980; Mathern et al., 1992). However, an alternate possibility is that spontaneous limbic seizures could alter glutamate receptor subunits. Recent studies indicate that following acute reactive seizures, ionotropic glutamate receptor mRNA levels change within minutes to hours, remain altered for hours to days, and occur in the absence axon sprouting (Gall et al., 1990; Kamphuis et al., 1992; Friedman et al., 1994; Gold et al., 1996; Lason et al., 1997). It is therefore unclear whether chronic limbic seizures show alterations in glutamate receptor subunits similar to those observed after acute reactive seizures and/or whether the changes in ionotropic glutamate receptor subunits correlate with aberrant mossy fiber sprouting.

In rats with spontaneous limbic seizures, this study determined if hippocampal AMPA and NMDA receptor subunit mRNA levels correlated with supragranular mossy fiber sprouting. We selected the pilocarpine status model because it shows fascia dentata mossy fiber sprouting similar to temporal lobe epilepsy patients and has a predictable time course of chronic seizures that replicates the human limbic epilepsy syndrome (for review, see Weiser et al., 1993; Mathern, 1998a). Following status epilepticus, animals enter a latent phase during which no spontaneous limbic seizures are observed. After 2 to 3 weeks, status rats begin to show spontaneous limbic seizures that progressively increase in number and severity until a plateau is reached. Thereafter, their limbic epilepsy is chronic and stable. By using this model, time-dependent changes can be monitored as animals progress through the various seizure phases. Results of this study have been presented in abstract form (Mathern et al., 1998c).

MATERIALS AND METHODS

Animal Preparation

This experiment was performed with approved institutional animal research protocols. Male Sprague-Dawley rats (150–200 g) were premedicated with methylscopolamine nitrate (1 mg/kg; s.q.) followed 30 minutes later by pilocarpine hydrochloride (320 mg/kg; i.p; Sigma, St. Louis, MO). A total of 53 rats were injected with pilocarpine; for the next 8–10 hours they were continuously observed for behavioral signs of status epilepticus (sustained motor seizures, unresponsiveness, facial clonus, etc.). Rats in status epilepticus for more than 6 hours were treated with a single dose of phenobarbital (1–2 mg; i.p.) to terminate the convulsions (pilocarpine status group). Controls consisted of naive rats injected with vehicle (naive controls; $n = 12$) and animals injected with pilocarpine but without signs of status (pilocarpine without [w/o] status; $n = 12$). The pilocarpine w/o status rats did not receive phenobarbital at 6 hours, and no medications were used to treat the chronic limbic seizures (see below).

All pilocarpine and control animals were prepared within 2–3 days and sacrificed at progressively greater time points based on the presence or absence of spontaneous limbic seizures and time after status. Pilocarpine status, pilocarpine w/o status, and naive control rats were monitored on average 4 hours per day, 5 days per week for behavioral signs of limbic seizures (prolonged staring, facial clonus, drooling, and/or secondary generalized seizures). Rats were perfused at the following time intervals defined by prior studies showing a sequential

evolution of the chronic limbic seizures (Leite et al., 1990; Cavalheiro et al., 1991; Bertram and Cornett, 1993, 1994; Mathern et al., 1993; Lemos and Cavalheiro, 1995): (1) during the **latent** phase (11 days poststatus; n = 7) after status-induced neuronal loss but before spontaneous limbic seizures begin; (2) in the **early** seizure phase after their first brief spontaneous limbic events (25 days poststatus; n = 7); and (3) in the **chronic** phase when the animals display repeated random limbic seizures (85 days poststatus; n = 9). The latent rats were randomly chosen from the pool of pilocarpine status animals; none of these rats were observed to have limbic seizures. The early seizure rats were those with at least one behavioral limbic seizure by day 25 poststatus; all of the chronic seizure rats had many witnessed limbic seizures days to weeks prior to sacrifice. Pilocarpine status rats without spontaneous limbic seizures were not sampled in the early and chronic seizure phases, and rats were observed 3 to 4 hours prior to sacrifice to ensure they had no seizures immediately before perfusion. Furthermore, none of the naive controls or pilocarpine w/o status animals had witnessed spontaneous seizures. Rats were sacrificed in batches (n = 4 to 5) consisting of control animals (naive and pilocarpine w/o status; n = 1 to 2) matched with pilocarpine status rats (n = 2 to 3) from either the latent, early seizure, or chronic seizure time periods.

Tissue Processing

Each batched set of rats were deeply anesthetized (pentobarbital; 50–75 mg per animal) and perfused via an aortic cannula with buffered normal saline for 1 min, 0.1% sodium sulphide in Millonig's buffer (pH 7.3) for 5 min, and buffered 4% paraformaldehyde for 5–10 min (Mathern et al., 1993, 1997a, 1998a). The brains were removed from the cranium, blocked, postfixed the first night, cryoprotected the second night (10% sucrose in 0.12 M phosphate buffer; pH 7.3), and quick-frozen and sectioned on a cryostat (−15°C) in the horizontal plane from the ventral brain surface. Adjacent sections, beginning at the level of the anterior commissure (ventral level), were collected for Nissl stain (10 μm and 30 μm), neo-Timm's histochemistry (two sections at 30 μm), and in situ hybridization (five sections at 30 μm). The Nissl and neo-Timm's sections were mounted onto chromium-alum gelatin-coated slides, and in situ sections onto Superfrost/Plus slides. Serial sections were collected two more times (middle and dorsal levels) for a total of three sequential sites that bilaterally sampled the ventral to middle hippocampus (i.e., total of six right and left sample sites per animal). The rat ventral hippocampus was sampled because it is anatomically analogous to the human anterior pes hippocampus that shows the maximal damage in temporal lobe epilepsy patients (Babb et al., 1984a,b). The slides for in situ hybridization were immediately stored for later batch processing (−70°C), and specimens were protected from RNase contamination throughout the histologic processing. The dorsal hippocampus near the corpus callosum was not sampled, and the process of perfusion, fixation, and tissue processing followed a strict set of protocols to ensure uniform results.

Hippocampal Neuronal Counts and Area Measurements

As previously published, sections were stained with cresylecht violet (CV) for histopathologic review (30-μm-thick) and cell densitometry (10 μm; Babb et al., 1984a,b; Mathern et al., 1992, 1993, 1995b, 1997a, 1998a). Neuron counts were performed on both the right and left hippocampus at the three ventral to dorsal horizontal levels and averaged into single values per animal. Neuron counts were performed at 400× using grid morphometric techniques, and the counted hippocampal subfields were based on Lorente de Nó's (1934) classification. The subfields were the granule cells of the fascia dentata, CA4, CA3, CA1, stratum pyramidale, and subiculum neurons (see Fig. 1A). Hilar polymorph neurons were not counted in this study. An ocular grid consisting of 10 by 10 boxes was placed over the hippocampal region of interest. For the stratum pyramidale, the 20 boxes in sequential 2 by 2 box segments (104 × 1,040 μm area) that followed the laminar profile of neurons were selected, and all nuclei belonging to pyramids within this region counted except for those touching the superior and right edges of the grid. Typically, nearly all of any cornu ammonis subfield would be included in a single counted field. For the smaller granule cells, a linear 1 by 5 box (52 × 260 μm area) was used and the measure was repeated. Final neuron counts were calculated as the number of neurons per 1,000 μm^2. To ensure a uniform counting technique, two blinded individuals (DM, AL) collected this data.

The two-dimensional areas of the counted principal hippocampal subfields were obtained from an image analysis computer. The 10-μm Nissl sections (the same ones used for neuron counts) were imaged using a video monochrome charge-coupled device camera (CCD; Hamamatsu) attached to a Zeiss microscope and captured, averaged, and digitized using a frame grabber (Data Translation Quick Capture; average of 16 serially collected video frames) on a Macintosh computer (Model 8100/110). Once captured, the image was analyzed using image system software (NIH Image; v. 1.56; public domain). The operator outlined for the computer the same regions used for cell counts, and the areas (μm^2) were determined (see Fig. 1A). For the stratum granulosum, the outline followed the granule cells over the upper and lower blades. The stratum granulosum and pyramidale

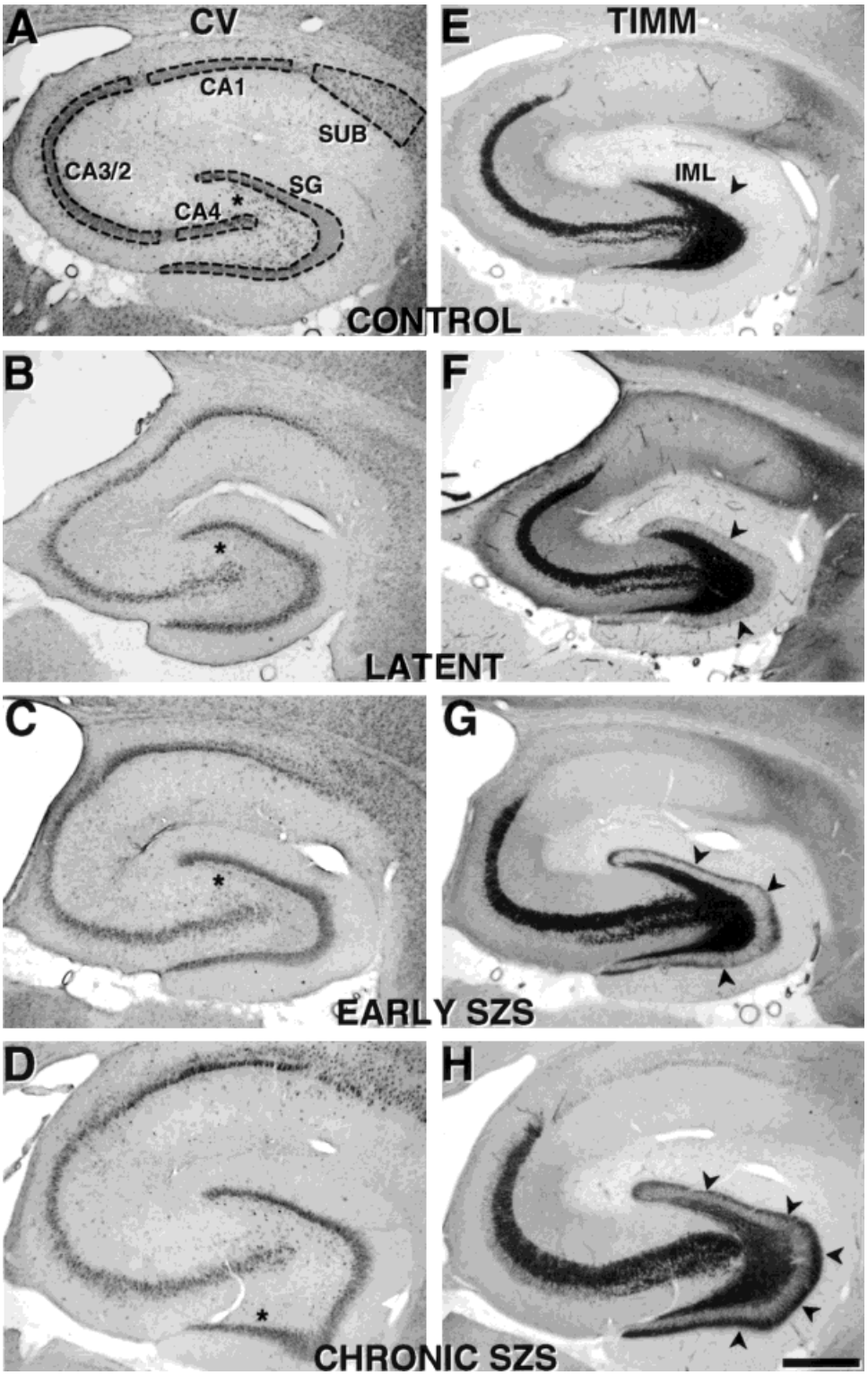

Fig. 1. Nissl (A–D) and neo-Timm's (E–H) sections from a naive control (**A** and **E**; 85-day-old rat), latent (**B** and **F**), early seizure (**C** and **G**), and chronic seizure rat (**D** and **H**). In A, the subfields used for neuronal counts and area measurements are indicated (dashed lines) and include the stratum granulosum (SG), CA4, CA3, CA1 stratum pyramidale, and subiculum (SUB). Compared with controls, all three pilocarpine status rats show hilar neuron loss (A–D, asterisks). Qualitatively, the hippocampal sizes were also different between pilocarpine status rats and controls. Compared with controls, latent phase animals had smaller hippocampi, while chronic seizure rats were more like controls or even slightly larger. Compared with controls, pilocarpine status rats showed progressively greater neo-Timm's staining in the inner molecular layer (IML; E–H, arrowheads). All panels at equal magnification. Calibration bar = 500 μm.

area measures from all six hippocampal sample sites were averaged into single values per animal.

It should be emphasized that neuron counting and area measures, as used in this study, are relative estimates and not absolute calculations of the number of neurons or size of hippocampal structures. However, our measures can be considered reliable relative estimates, statistical differences between groups of animals that are similarly processed can be accurately determined, and our method is an accepted quantitative technique in animal hippocampal studies (Bertram et al., 1990; Bertram and Lothman, 1993; Mathern et al., 1992, 1993, 1997a, 1998a; Leite et al., 1996).

Neo-Timm's Histochemistry and Inner Molecular Layer Staining

This procedure was the same as previously published (Babb et al., 1991; Mathern et al., 1992, 1993, 1995c, 1997a, 1998a). Briefly, two sets of adjacent 30-µm sections, one developed lightly and the other darkly, were processed to confirm that the staining was specific for mossy fibers. The slides were immersed in a ''physical developer'' maintained at 26°C in the darkroom. The developer consisted of 180 ml of a 50% gum arabic solution, 30 ml of an aqueous solution of 7.65 g citric acid and 7.05 g sodium citrate, 90 ml of an aqueous solution of 5.3 g hydroquinone, and 1.5 ml of a 17% silver nitrate solution. Development time for light sections was 30 min and for dark sections was 40 min. The slides were washed in distilled water for 5 min and running tap water for 10 min, air-dried, dehydrated through alcohol to xylene, and coverslipped.

The optical density (darkness) of inner molecular layer staining was measured as the average of the gray values (GV) between white (0) to black (255), as previously published (Mathern et al., 1995a, 1996, 1997a, Leite et al., 1996). The neo-Timm's sections were imaged using the same computer system as the area measurements. Illuminance was uniformly maintained and checked after every 10 measurements using optical density standards (Kodak, Rochester, NY). The operator imaged the fascia dentata molecular layer between the hippocampal fissure to the stratum granulosum and outlined the inner molecular layer (IML). The computer determined the average GV of the pixels within the encircled region. Measurements were performed on the right and left hippocampi of the darkly stained sections at each of the three horizontal levels and averaged into single values per animal.

Riboprobe Preparation

Full-length cDNA constructs of rat AMPA and NMDA receptor subunits (courtesy of the Salk Institute and Dr. Jim Boulter; Boulter et al., 1990) included GluR1 (p59/2), GluR2 (pRB14), GluR3 (pRB312), NMDAR1-1a (pNMDAR1-1a), and NMDAR2b (pJS2B) clones. The cDNAs were subcloned into the EcoR1 site of the Bluescript plasmid vector. Plasmid cDNAs were linearized with EcoR1 (GluR1), Not I (GluR2, GluR3), BamH I (NMDAR1), or Hind III (NMDAR2b). Full-length antisense cRNAs were transcribed with T7 (GluR1, 2, 3, and NMDAR1) or T3 (NMDAR2b) RNA polymerase in the presence of ^{35}S-UTP (Dupont, Boston, MA). Prior studies indicate that these AMPA and NMDA mRNA constructs do not cross-hybridize to other glutamate receptor subunits (Boulter et al., 1990; Gold et al., 1996). All enzymes were supplied by Stratagene (La Jolla, CA).

In Situ Hybridization

In situ hybridization procedures were performed as a batch process for each riboprobe and followed previously published protocols (Gall and Isackson, 1989; Kornblum et al., 1994; Mathern et al., 1997b). Briefly, slides with sections adjacent to the ones used for neuron counts were removed from storage (−70°C) and warmed under a stream of cool air to avoid condensation. Once at room temperature, sections were pretreated with 0.1 M glycine in 0.1 M phosphate buffer (PB, pH 7.4, 0.25% acetic anhydride in 0.1 M triethanolamine (pH 8.0), and washes of 2× standard saline citrate (SSC). Slides were dehydrated through graded ethanols, immersed in chloroform (5 min), rehydrated, and air-dried. Hybridization was performed at 60°C for 18–24 hours using approximately 250 µl of hybridization solution per slide (consisting of the three ventral to dorsal sections per animal) consisting of 50% formamide, 10% dextran sulfate, 0.65% ficoll, 0.65% polyvinyl pyrrolidone, 0.65% bovine serum albumin, 0.15 mg/ml yeast transfer RNA, 0.3 mg/ml denatured salmon sperm DNA, 40 mM DTT, and ^{35}S-labeled cRNA probe at a concentration of 1×10^7 cpm/ml of hybridization solution. The next day, sections were washed twice at 60°C in 4× SSC and 10 mM sodium thiosulfate (STS; 25 min each) and treated at 45°C with 20 µg/ml ribonuclease A in 0.5 M NaCl/10 mM Tris (pH 8.0)/1 mM EDTA (40 min). Slides were washed for 25 min in SSC/STS of decreasing SSC concentration starting with four washes at room temperature in 2× SSC/10 mM STS, two washes at 60°C in 0.5× SSC/10 mM STS, one wash at 60°C in 0.1× SSC/10 mM STS, and one wash at room temperature in 0.1× SSC/10 mM STS. The slides were rinsed in de-ionized autoclaved water and air-dried. In situ controls consisted of tissue sections initially treated with RNase.

In Situ Autoradiography and Densitometric Analysis

Hybridization densities over principal hippocampal subfields were visualized by film (Amersham, Arlington

Heights, IL; Beta Max) and emulsion (Kodak, NTB2) autoradiography and quantified using image analysis techniques (Gold et al., 1996; Mathern et al., 1997b). Slides were placed in film cassettes and exposed for 5 days. The film was developed in D19 (Kodak, 1:1 dilution, 4 min); rinsed 30 sec in distilled water, KodaFix (Kodak 1:3 dilution, 10 min), and running water for 20 min; and air-dried. After film autoradiography, the slides were dehydrated through graded ethanols, immersed in chloroform (20 min), rehydrated to 50% ethanol, air-dried, and dipped for emulsion autoradiography (Kodak NTB2, 1:1 dilution). Exposure time averaged 4 to 5 weeks; slides were developed in Kodak D19 and Kodak fixer and counterstained (cresylecht violet).

Hybridization densities were measured from the film autoradiographs by another image analysis computer using the same anatomic landmarks and subfield nomenclature as the cell counts (Olympus Microscope and MCID Imaging Software; Imaging Research, Inc.; Ontario). Briefly, the operator outlined for the computer the fascia dentata stratum granulosum and pyramidale based on previously prepared copies of the adjacent Nissl-stained sections used for cell counts, and the computer determined the optical density of silver grains. Hybridization densities were calibrated relative to ^{14}C-radiolabeled standards (American Radiolabeled Chemical, Inc., St. Louis, MO), and the range of tissue hybridization densities occupied the linear portion of the exposure/density curve (of known cpm/protein content). Measurements were performed on the right and left hippocampus at each of the three horizontal levels and averaged into single values per animal.

Data Analysis

Data was entered into a database on a personal computer and analyzed using a statistical program (Super ANOVA Version 1.1, Abacus Concepts, Inc., Berkeley, CA). Differences between controls and pilocarpine status rats from the latent, early seizure, and chronic seizure phases were statistically compared using an analysis of variance (ANOVA) and further compared between individual categories (at $P < 0.05$) using Scheffe's post-hoc tests. Other statistical tests included the analysis of covariance (ANCOVA) and regression analyses. Results were plotted with DeltaGraph Professional (DeltaPoint, Inc., Monterey, CA) and considered significantly different at a minimum confidence level of $P < 0.05$.

RESULTS

Control Comparisons

As a first analysis, we determined if naive and pilocarpine w/o status rats showed differences in hippocampal neuron counts, area measures, and AMPA and NMDA hybridization densities. There were 12 naive control animals killed during the latent (n = 3), early seizure (n = 5), and chronic seizure time periods (n = 4) and 12 pilocarpine w/o status rats studied during the latent (n = 3), early seizure (n = 4), and chronic seizure phases (n = 5). Naive controls and pilocarpine w/o status rats showed no significant differences in hippocampal neuron counts (t-tests; $P > 0.58$), stratum granulosum and pyramidale area measurements ($P > 0.16$), IML neo-Timm's GV ($P = 0.27$), and averaged GluR1–3 and NMDAR1–2b hybridization densities ($P > 0.16$). Furthermore, after pooling the naive and pilocarpine w/o status animals, there were no differences between animals sacrificed during the latent (day 11), early seizure (day 25), and chronic seizure (day 85) time periods for averaged hippocampal GluR1–3 and NMDAR1–2b hybridization densities (ANOVAs; $P > 0.23$). Based on these findings, the naive and pilocarpine w/o status rats were combined into a single control category for comparison with the pilocarpine status animals killed during the different poststatus time periods.

Hippocampal Neuron Counts and IML Neo-Timm's Staining

Nissl sections and neuron loss. Compared with controls, pilocarpine status rats showed hilar cell loss, minimal neuronal loss in other hippocampal subfields, and a slight change in stratum pyramidale size (Figs. 1 and 2). By visual inspection, all pilocarpine status rats showed hilar neuron loss compared with controls (Fig. 1A–D, asterisks). Of note, the hilus was not one of the quantitatively counted subfields (see outlines Figs. 1A and 2). Depending on the time after pilocarpine status, there were also visual differences in hippocampal size. Compared with controls, hippocampi from latent phase rats were often smaller than expected (Fig. 1B) and chronic seizure hippocampi were occasionally larger (Fig. 1D). Closer inspection disclosed that most of the size differences were from changes in dendritic thickness, especially in the CA3 and CA1 stratum radiatum. By comparison, the stratum granulosum and pyramidale areas were only minimally different. In other words, pilocarpine status rats showed minimal visible hippocampal neuron loss, except for hilar cells.

Figure 2 shows the mean (±S.E.M.) neuron counts for controls and pilocarpine status rats (upper left), and the data follows the qualitative observations (Fig. 1). Compared with controls, chronic and early seizure rats showed decreased stratum granulosum (SG; −6% and −11%, respectively), CA4 (−19% and −30%), CA3 (−10% and −20%), and CA1 (−12% and −25%) neuron densities (ANOVAs; $P < 0.0003$; see asterisks, Fig. 2). By comparison, the subiculum neuron densities were

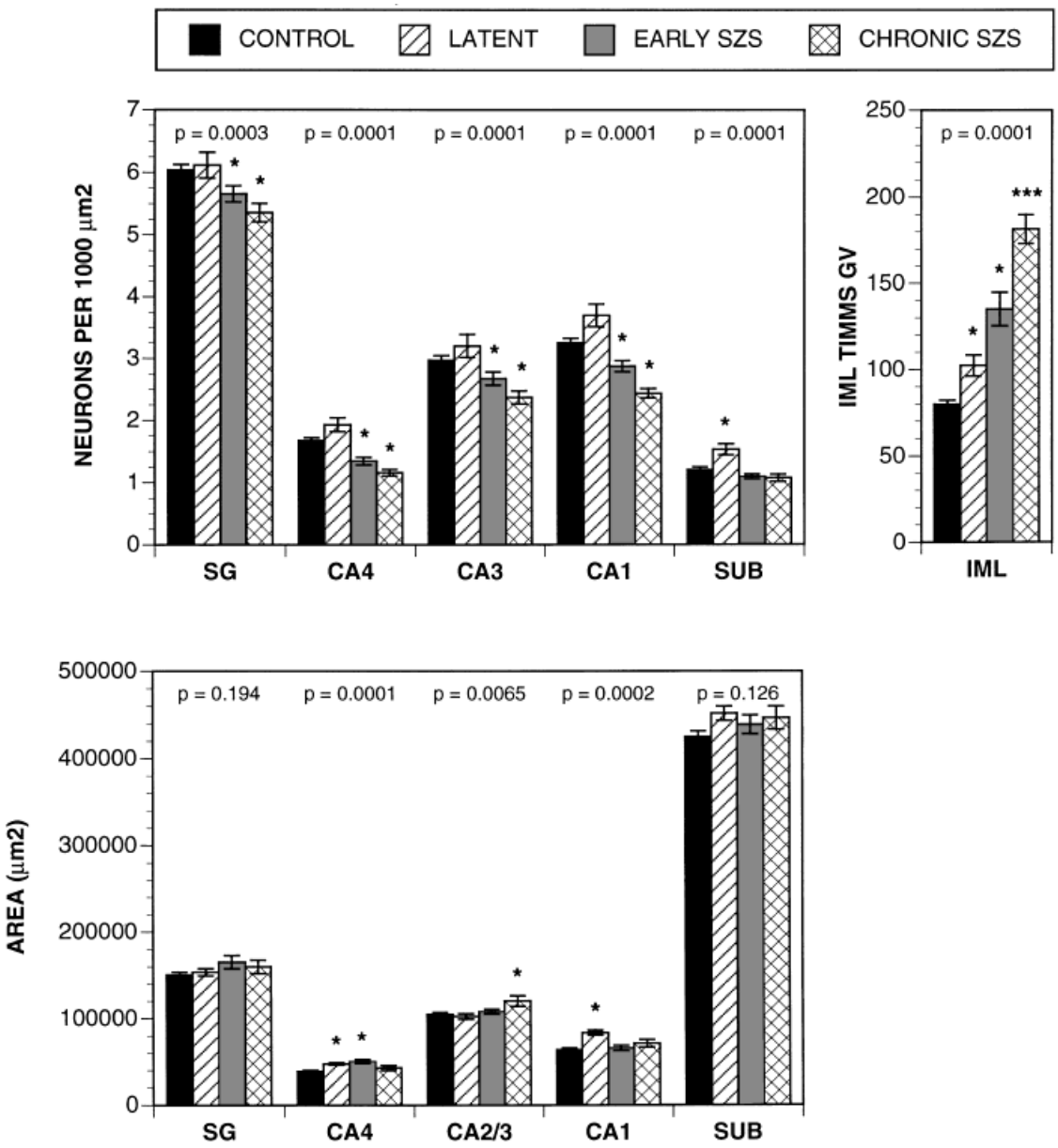

Fig. 2. Histograms showing the mean (±S.E.M.) neurons/µm^2 (**upper left**), principal subfield area measurements (µm^2, **lower**), and inner molecular layer (IML) neo-Timm's staining (gray values [GVs], **upper right**) for controls, latent, early seizure (early szs), and chronic seizure rats (chronic szs). The analysis of variance (ANOVA) *P*-values are shown above each subfield, and significant post-hoc differences indicated by asterisks ($P < 0.05$). A single asterisk indicates a difference compared with controls, and multiple asterisks indicate differences compared with controls and one or more of the other pilocarpine status groups. Neuron counts: significant post-hoc tests, compared with controls, showed that early and chronic seizure rats had decreased neuron counts in the: (1) SG ($P < 0.0008$); (2) CA4 ($P < 0.0004$); (3) CA3 ($P < 0.009$); and (4) CA1 subfield ($P < 0.011$). By comparison, the subiculum showed an increase in counts for latent rats compared with controls ($P = 0.0002$). Area measures: Significant post-hoc tests, compared with controls, showed increased areas for the: (1) CA4 region of latent and early seizure rats ($P < 0.002$); (2) CA2/3 subfields of chronic seizure rats ($P = 0.0013$); and (3) CA1 region of latent rats ($P = 0.0001$). IML Timm's: Compared with controls, IML GVs were increased in latent ($P = 0.042$), early seizure ($P = 0.0001$), and chronic seizure animals ($P = 0.0001$).

increased in latent phase animals (+27%). There were also small but statistically significant differences in the two-dimensional size of hippocampal cell layers (Fig. 2, lower graph). Compared with controls, the following principle cell areas were increased: (1) CA4 stratum pyramidale for latent and early seizure rats (area between SG blades; +22% and +29%, respectively); (2) CA2/3 stratum pyramidale for chronic seizure animals (+15%);

and (3) CA1 stratum pyramidale for latent phase animals (+31%; $P < 0.0065$, see asterisks, Fig. 2). By comparison, the stratum granulosum and subiculum showed no differences in areas measurements between controls and pilocarpine-status rats ($P > 0.126$).

Collectively, the data indicates that following pilocarpine status, CA4 and CA1 stratum pyramidale areas were often transiently increased during the latent and early seizure phases. In addition, there were decreased neuron densities in many hippocampal subfields of early and chronic seizure rats. Hence, the number of granule cells and CA4 and CA1 pyramids were probably reduced in early and chronic pilocarpine status rats compared with controls. By comparison, in CA2/3 stratum pyramidale and subiculum, it is unclear if chronic seizure animals showed neuron loss or a change in hippocampal size with secondary alterations in neuron densities.

Neo-Timm's IML staining. Pilocarpine status rats showed IML neo-Timm's staining that increased with longer survivals (Fig. 1E–H, arrowheads). This is consistent with prior studies of other poststatus rat models (Mathern et al., 1992, 1993, 1998a; Okazaki et al., 1995). By comparison, none of the naive controls or pilocarpine w/o status animals demonstrated IML neo-Timm's staining (Fig. 1E). Neo-Timm's GV measurements confirmed that IML staining progressively increased with time (Fig. 2, upper right). Compared with controls, IML GVs increased in latent (+28%), early seizure (+69%), and chronic seizure rats (+127%; see asterisks, Fig. 1).

AMPA and NMDA mRNA Hybridization Densities

The same control, latent, early seizure, and chronic seizure rats presented in the Nissl and neo-Timm's illustrations were used to show mRNA changes (Figs. 3–5). Darkfields include GluR1, GluR2 (Fig. 3), GluR3 (Fig. 4), NMDAR1, and NMDAR2b (Fig. 5), and Figure 6 illustrates the quantitative hybridization densities (mean ± S.E.M.). In summary, there were statistically significant differences in hippocampal AMPA and NMDA subunit hybridization densities between controls and pilocarpine-status rats over the different time-dependent and seizure phases. Changes such as stratum granulosum GluR3 mRNA levels (Fig. 4) paralleled increased neo-Timm's mossy fiber sprouting (Fig. 1), while other mRNA alterations were related to the poststatus seizure phase (Fig. 6). Of note, our long-term poststatus hippocampal mRNA changes were generally less than 40% of controls values. This is smaller in number than the 50% to 150% changes often reported for the same subunits after acute reactive limbic seizures or status epilepticus (see Discussion).

GluR1 mRNA levels. Hippocampal GluR1 hybridization densities showed minimal differences between control and pilocarpine-status rats. In control animals, GluR1 densities were fairly evenly distributed between the stratum granulosum and pyramidale, and there were clusters of silver grains over hilar neurons (Fig. 3A). Hilar silver grain clusters were observed less frequently in latent, early seizure, and chronic seizure rats (Fig. 3B–D, asterisks) consistent with hilar neuron loss (Fig. 1A–D, asterisks). In chronic seizure rats and relative to CA1 stratum pyramidale, subiculum hybridization densities were slightly decreased (Fig. 3A–D, arrowheads); this was supported by the quantitative measurements (Fig. 6). Compared with controls, latent (−23%) and chronic seizure rats (−16%) showed decreased subiculum GluR1 mRNA levels.

GluR2 mRNA levels. Compared with controls (Fig. 6), chronic seizure animals showed: (1) increased fascia dentata (FD) GluR2 hybridization densities (+13%) and (2) decreased CA1 and subiculum mRNA levels (−18% and −31%, respectively). These findings are visually illustrated in Figure 3 (E–H). CA1 and subiculum hybridization densities were decreased in chronic seizure rats compared with controls (Fig. 3E–H, arrowheads). Likewise, stratum granulosum GluR2 hybridization densities were increased in chronic seizure rats compared with controls (Fig. 3H, arrows). Finally, hilar GluR2 silver grain clusters were reduced in all pilocarpine status rats (Fig. 3E–H, asterisks).

GluR3 mRNA levels. Stratum granulosum GluR3 hybridization densities increased with longer poststatus survivals similar to the increase in supragranular mossy fiber sprouting (Figs. 1E–H and 4). Visually, all three pilocarpine status rats showed increased stratum granulosum GluR3 hybridization densities compared with controls (Fig. 4A–D, arrowheads; 4E–H). This was most prominent in latent (Fig. 4B and F) and chronic (Fig. 4D and H) pilocarpine status rats. Furthermore, there were increased CA4 and CA3 GluR3 hybridization densities in chronic seizure rats compared with controls (Fig. 4D, arrows). As expected, hilar GluR3 silver grain clusters were decreased in all pilocarpine status rats (Fig. 4A–D, asterisks). The visual and quantitative findings were similar (Fig. 6). Compared with controls: (1) latent (+38%), early (+24%), and chronic (+53%) rats showed increased FD GluR3 hybridization densities and (2) chronic seizure rats demonstrated increased CA4 and CA3 stratum pyramidale mRNA levels (+23 and +17%, respectively).

NMDAR1 mRNA levels. Following pilocarpine status, there was a visible increase in NMDAR1 hybridization densities over the stratum granulosum and CA4 and CA1 stratum pyramidale in latent phase rats compared with controls (Fig. 5A–B, arrowheads). In early seizure rats, NMDAR1 mRNA densities in the same subfields were less than latent animals, but still greater than controls (Fig. 5C, arrowheads). Finally, chronic

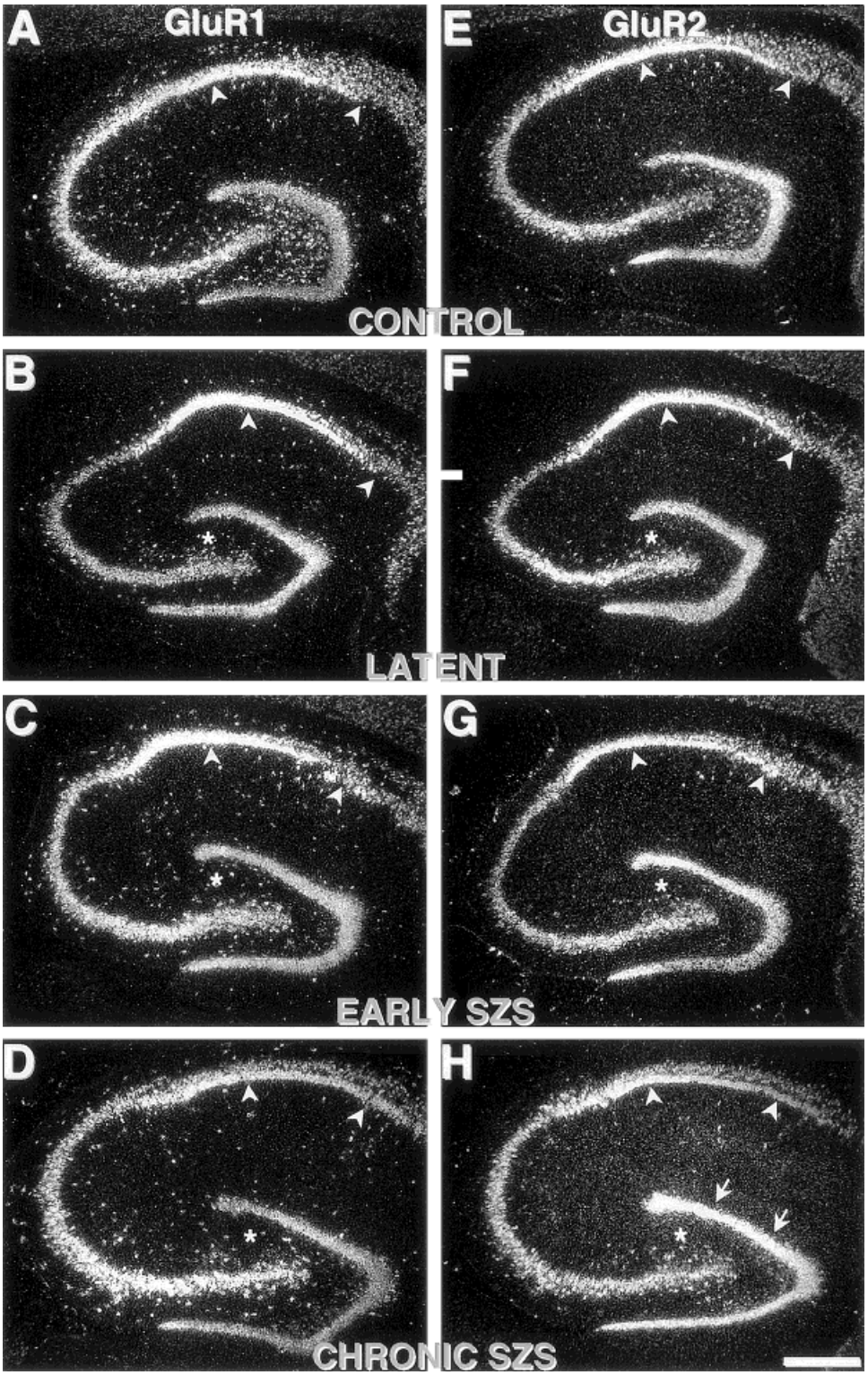

Fig. 3. Darkfield autoradiographs of GluR1 (**A–D**) and GluR2 (**E–H**) hybridization densities from the same rats illustrated in Figure 1. For GluR1 and GluR2, there is a loss of hilar silver grain clusters in all pilocarpine status rats compared with controls (asterisks). In addition, there are decreased CA1 and subiculum GluR1 hybridization densities in chronic seizure rats compared with the controls and latent phase animals (A–D, arrowheads). The decrease in regio superior mRNA levels is more evident for GluR2 compared with GluR1. Calibration bar = 500 μm.

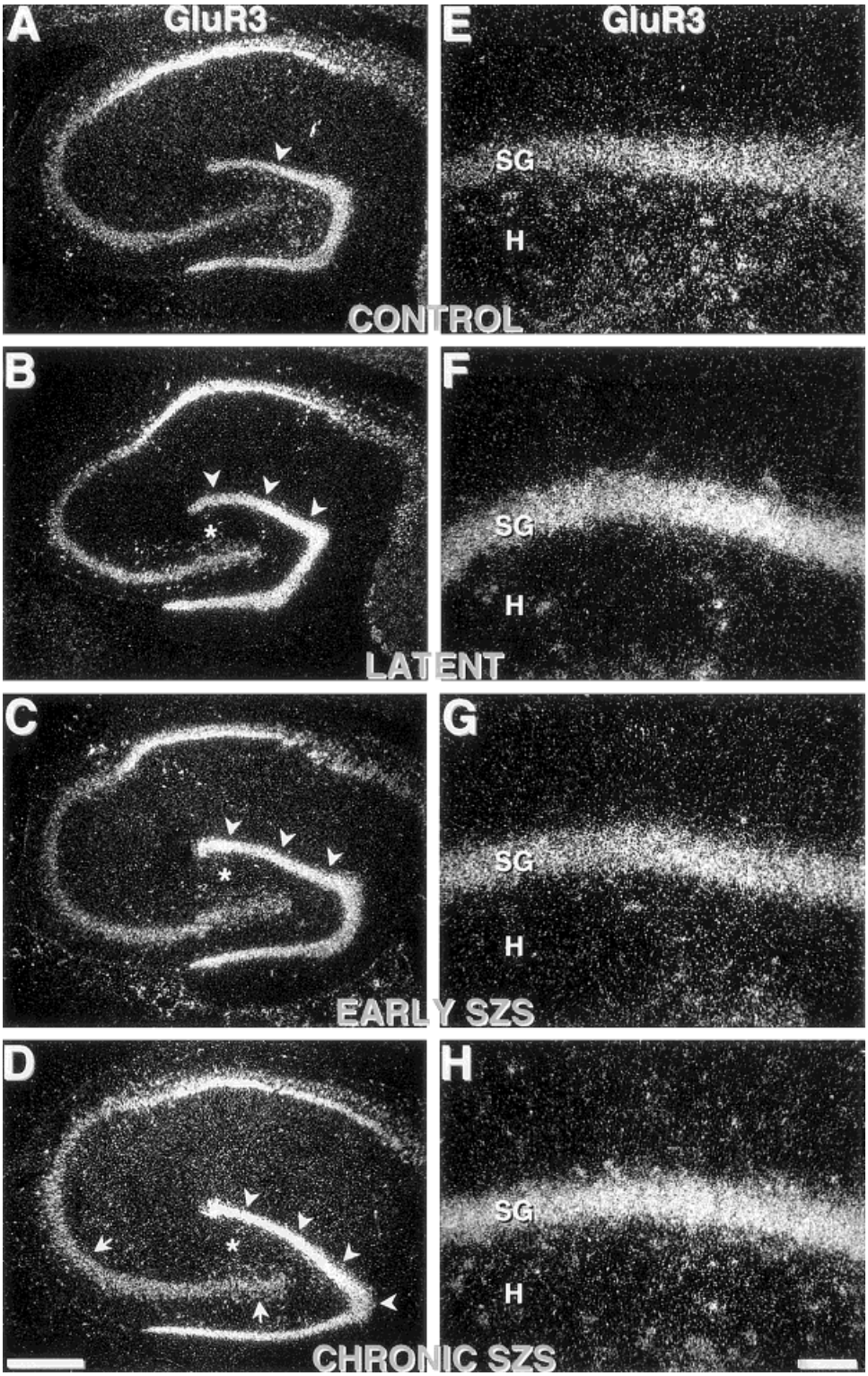

Fig. 4. Darkfields for GluR3 from the same rats as Figure 1 and 3 (**A–D**), and magnified views of the fascia dentata stratum granulosum (SG; **E–H**). The magnified views are oriented with the hilus (H) at the bottom of the panel. Compared with controls, there are increased stratum granulosum GluR3 hybridization densities in the latent, early seizure, and chronic seizure rats (arrowheads). In addition, the chronic seizure rat shows greater GluR3 hybridization densities in CA4 and CA3 compared with controls (D, arrows). Lastly, there is loss of hilar silver grain clusters in all pilocarpine status rats (asterisks). Calibration bars = 500 μm for A–D; 100 μm for E–H.

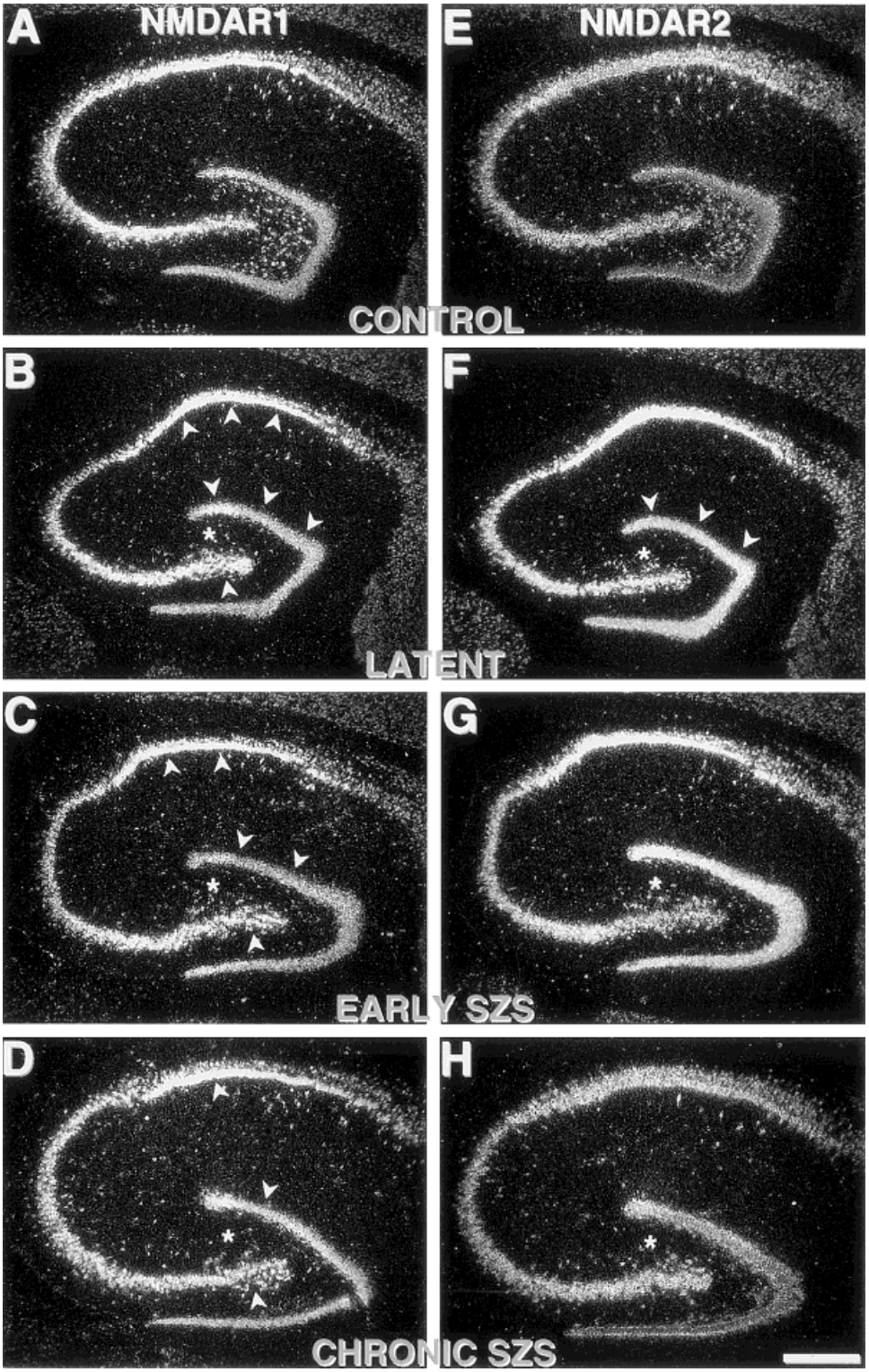

Fig. 5. Darkfields for NMDAR1 (A–D) and NMDAR2b (E–H). Compared with controls, latent phase rats showed increased NMDAR1 hybridization densities over the stratum granulosum, CA4, and CA1 stratum pyramidale (arrowheads). Early seizure animals showed NMDAR1 mRNA levels were less than latent rats, and returned to control levels in chronic seizure animals (arrowheads). For NMDAR2b, there were increased stratum granulosum densities during the latent phase compared with controls (arrowheads). In addition, for both NMDAR1 and NMDAR2b, hilar silver grain clusters were decreased in pilocarpine status rats compared with controls (asterisks). Calibration bar = 500 μm.

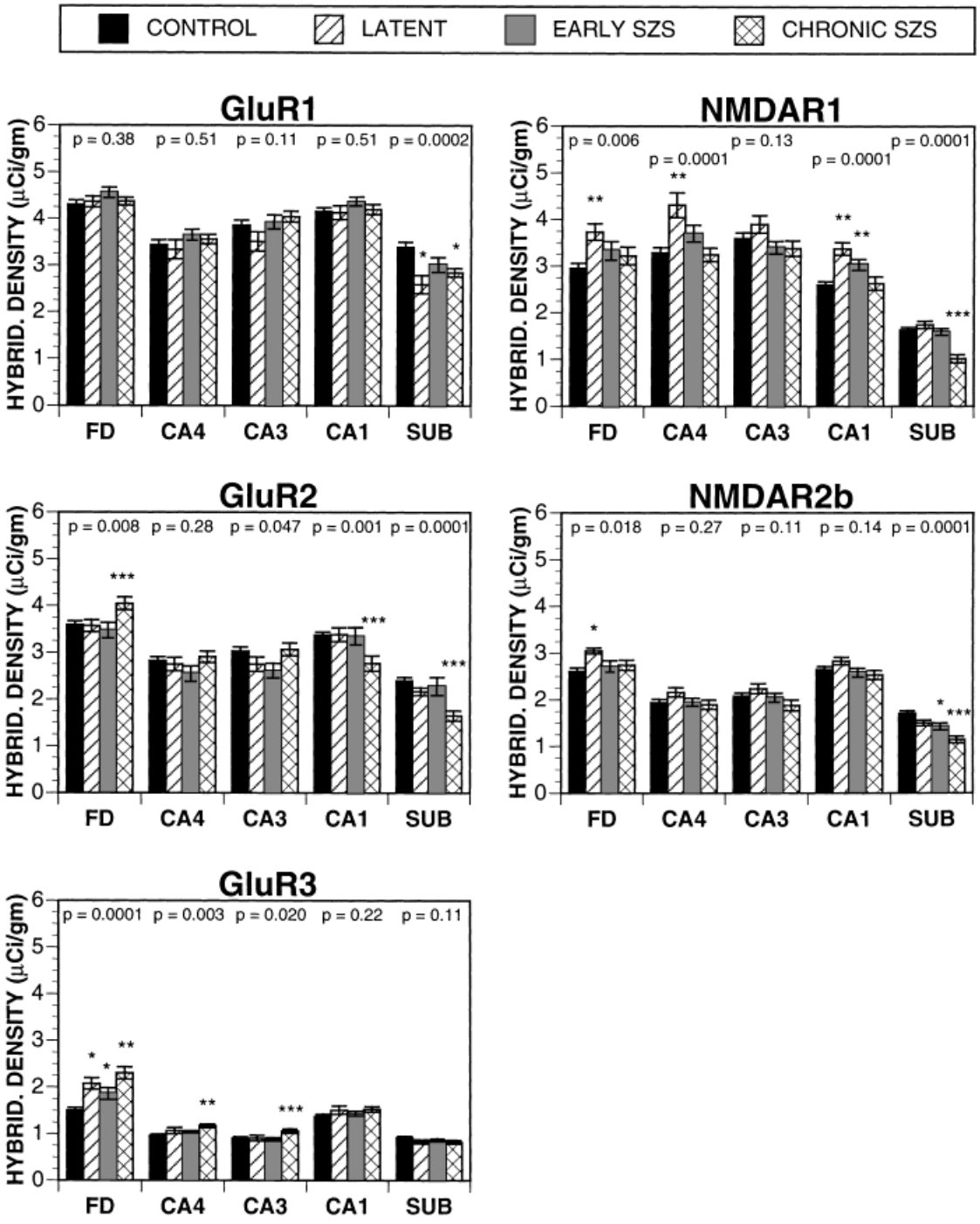

Fig. 6. Histograms showing the mean (±S.E.M.) hybridization densities for GluR1–3 and NMDAR1–2b for pilocarpine status rats. GluR1: The subiculum mRNA levels of latent and chronic seizure rats were less than controls ($P < 0.003$). GluR2: (1) The fascia dentata (FD) mRNA levels of chronic rats were greater than controls ($P = 0.0035$) and the other pilocarpine status groups ($P < 0.012$); and (2) the CA1 and subiculum subfields mRNA levels of chronic seizure rats were less than controls ($P < 0.0003$) and the other two pilocarpine status groups ($P < 0.004$). GluR3: (1) The FD mRNA levels of latent and early seizure rats were greater than controls ($P < 0.011$), and chronic seizure rats were greater than controls ($P = 0.0001$) and early seizure rats ($P = 0.0058$); and (2) the CA4 and CA3 mRNA levels of chronic seizure rats were greater than controls ($P < 0.0052$) and one or more of the other pilocarpine status groups ($P < 0.045$). NMDAR1: (1) The FD and CA4 mRNA levels of latent rats were greater than controls ($P < 0.0006$) and chronic seizure rats ($P < 0.040$); (2) the CA1 mRNA levels of latent and early seizure rats were greater than controls ($P < 0.0047$) and chronic seizure animals ($P < 0.019$); and (3) the subiculum mRNA levels of chronic seizure rats were less than the other three groups ($P = 0.0001$). NMDAR2b: (1) The FD mRNA levels of latent animals were greater than controls ($P = 0.0017$); and (2) the subiculum mRNA levels of early seizure rats were less than controls ($P < 0.021$), and chronic seizure rats were less than the other three groups ($P < 0.010$).

TABLE I. Multivariate Analysis of Covariance (ANCOVA) Comparing the Rat Time Course Categories (Category), Neuronal Densities (Counts), Neuronal Area (Area), and Inner Molecular Layer (IML) Neo-Timm's Gray Values (GVs; IML stain) to alpha amino-3-hydroxy-5-methyl-4-isoxazole-propionate (AMPA) and n-methyl-D-aspartic acid (NMDA) Receptor Subunit Hybridization Densities*

Subunit	Granule cells	CA4 pyramids	CA3 pyramids	CA1 pyramids	Subiculum
GluR1					
Category	3.01/.057	1.04/.376	1.96/.125	2.58/.058	**3.00/.034**
Counts	.418/.519	.004/.951	.907/.343	.913/.341	**8.74/.004**
Area	**6.65/.011**	.164/.687	1.05/.309	.079/.779	2.60/.109
IML stain	2.50/.117	2.49/.118	3.12/.080	**11.2/.0011**	**14.0/.0003**
GluR2					
Category	**3.96/.010**	1.81/149	**3.89/.011**	.893/.448	2.29/.082
Counts	1.75/.188	.547/.461	.684/.410	.552/.503	.549/.460
Area	1.09/.298	3.39/.068	.908/.343	2.04/.156	1.55/.216
IML stain	.061/.805	1.23/.270	.645/.424	**9.07/.0032**	**5.73/.018**
GluR3					
Category	**8.02/.0001**	**3.06/.031**	2.04/.112	1.84/.144	.422/.738
Counts	2.26/.136	.964/.328	2.05/.155	.052/.820	**4.62/.034**
Area	.142/.707	1.41/.238	3.64/.059	1.35/.247	**4.33/.039**
IML stain	**7.82/.0062**	.021/.886	.002/.964	.871/.353	2.96/.088
NMDAR1					
Category	**4.29/.0068**	4.70/.004	2.16/.098	**8.37/.0001**	6.24/.0006
Counts	.604/.439	.884/.349	.939/.335	.135/.714	.473/.493
Area	.063/.803	1.28/.260	.150/.699	1.10/.296	1.03/.313
IML stain	**6.51/.0123**	.083/.774	.311/.578	2.79/.098	3.45/.066
NMDAR2b					
Category	**3.53/.0177**	.797/.498	.510/.676	.458/.712	**4.21/.0078**
Counts	2.78/.098	2.34/.129	.714/.399	.098/.754	1.69/.197
Area	**3.99/.048**	3.29/.072	.960/.329	.542/.463	**5.83/.017**
IML stain	1.75/.188	.157/.693	.064/.801	1.87/.174	1.96/.164

*Data presented as F values/*P* values, and significant results indicated in bold type. There were no statistically significant interactions.

seizure rats showed NMDAR1 hybridization densities similar to controls (Fig. 5D, arrowheads). In addition, there was loss of hilar NMDAR1 silver grain clusters in all pilocarpine-status rats (Fig. 5A–D, asterisks). Quantitative measurements concurred with the visual observations (Fig. 6). Compared with controls: (1) latent phase rats showed increased NMDAR1 hybridization densities over the FD and CA4 subfields (+26% and +31%, respectively); (2) latent and early seizure animals demonstrated increased CA1 stratum pyramidale densities (+30% and +17%, respectively); and (3) chronic seizure rats showed decreased subiculum densities (−38%).

NMDAR2b mRNA levels. There were minimal differences in NMDAR2b hybridization densities between controls and pilocarpine status rats. Compared with controls, latent phase rats showed increased stratum granulosum NMDAR2b hybridization densities (Fig. 5F, arrowheads). Otherwise, there were no other obvious differences, except for the loss of hilar silver grain clusters in all pilocarpine-status rats (Figs. 5E–H, asterisks). This was supported by the quantitative measurements that showed that compared with controls: (1) latent phase rats showed increased FD NMDAR2b hybridization densities (+17%) and (2) early (−17%) and chronic (−33%) pilocarpine status groups demonstrated decreased subiculum densities.

Multivariate Analyses and Correlations With IML Neo-Timm's Staining

Because there were differences between controls and pilocarpine status rats for neuron counts, area measures, and IML neo-Timm's staining (Figs. 1, 2), it was important to establish whether the time after status or the anatomic variables were associated with differences in hippocampal GluR1–3 and NMDAR1–2b mRNA levels (Figs. 3–6). To answer this question, we performed a ANCOVA; the results are shown in Table I. Of the 25 statistical comparisons, the pilocarpine status time course categories showed differences in glutamate receptor subunit hybridization densities in 11 (44%; Table I, top rows). In other words, comparisons between controls and pilocarpine status rats for hybridization densities without statistically considering neuron counts, areas, and IML neo-Timm's staining found 13 subfields to be different (Fig. 6), and 11 (85%) comparisons remained significantly different in the multivariate ANCOVA (Table I). Hence, the time after pilocarpine status and the presence

of spontaneous limbic seizures were important factors affecting AMPA and NMDA receptor subunit mRNA levels.

The multivariate analyses (Table I) also indicates that, in certain subfields, neuron counts, area measures, and IML neo-Timm's staining correlated with GluR1–3 and NMDAR1–2b hybridization densities. For neuron counts (Table I; second row), subiculum densities negatively correlated with GluR1 ($R = -0.435$; $P = 0.004$) and GluR3 ($R = -0.325$; $P = 0.034$) mRNA levels. For area measures (Table I, third row), stratum granulosum areas positively correlated with GluR1 ($R = +0.254$; $P = 0.011$) and NMDAR2b ($R = +0.344$; $P = 0.034$) mRNA levels. For area measures (Table I, third row), stratum granulosum areas positively correlated with GluR1 ($R = +0.254$; $P = 0.011$) and NMDAR2b ($R = +0.344$; $P = 0.048$) mRNA levels, and subiculum areas positively correlated with GluR3 ($R = +0.339$; $P = 0.039$) and NMDAR2b ($R = +0.484$; $P = 0.017$) hybridization densities. These were the only subfields where neuron counts ($n = 2$; 8%) and area measures ($n = 4$; 16%) were found to significantly correlate with AMPA and NMDA mRNA levels in the multivariate ANCOVA (Table I).

More importantly, in the multivariate analyses there were six (24%) correlations between IML neo-Timm's staining and AMPA and NMDA mRNA levels (see Table I, bottom row); they are illustrated in Figure 7. For granule cells (GC), IML neo-Timm's GVs positively correlated with GluR3 ($R = +0.580$; $P = 0.0062$) and NMDAR1 mRNA levels ($R = +0.315$; $P = 0.0123$; Fig. 7, top row). Furthermore, IML neo-Timm's GVs negatively correlated with CA1 and subiculum GluR1 ($R = -0.181$ and -0.337; $P = 0.0011$ and 0.0003, respectively; Fig. 7, middle row) and GluR2 hybridization densities ($R = -0.536$ and -0.562; $P = 0.0032$ and 0.018, respectively; Fig. 7, bottom row). The negative slopes were greater for GluR2 compared with GluR1 (Fig. 7, compare last two rows) and may explain why the time course comparisons failed to demonstrate decreased CA1 hybridization densities in chronic animals compared with controls (Figs. 3 and 6). As might be expected from the data in Figure 7, linear regression analyses found that IML neo-Timm's GVs correlated with GC GluR3 ($P = 0.0001$), GC NMDAR1 ($P = 0.045$), subiculum GluR1 ($P = 0.031$), CA1 GluR2 ($P = 0.0003$), and subiculum GluR2 ($P = 0.0001$) mRNA levels. However, CA1 GluR1 densities did not correlate with IML neo-Timm's GVs ($P = 0.28$) in linear regression analysis. In summary, multivariate ANCOVA analyses considering neuron counts, area measures, and time course categories showed that neo-Timm's mossy fiber sprouting correlated with increased granule cell GluR3 and NMDAR1 and decreased CA1 and subiculum GluR1 and GluR2 mRNA levels, and most of these mRNA changes began during the latent period prior to the onset of spontaneous limbic seizures.

DISCUSSION

This study compared hippocampi from controls (naive and pilocarpine w/o status rats) and pilocarpine status rats killed at successively longer time periods and found long-term changes in AMPA GluR1–3 and NMDAR1–2b hybridization densities (Figs. 1–6; Table I). Compared with controls, pilocarpine status rats sacrificed during the: (1) latent phase (day 11 poststatus) after neuronal injury but before spontaneous limbic seizures showed increased fascia dentata GluR3, NMDAR1, and NMDAR2b; increased CA4 and CA1 NMDAR1; and decreased subiculum GluR1 hybridization densities; (2) early seizure phase (day 25) after their first spontaneous seizures showed increased fascia dentata GluR3, increased CA1 NMDAR1, and decreased subiculum NMDAR2b mRNA levels; and (3) chronic seizure phase (day 85) when animals displayed recurrent limbic seizures showed increased fascia dentata GluR2; increased fascia dentata and CA4 GluR3; decreased CA1 GluR2; and decreased subiculum GluR1, GluR2, NMDAR1, and NMDAR2b hybridization densities. Furthermore, multivariate ANCOVA analyses showed that greater IML neo-Timm's GVs: (1) positively correlated with fascia dentata GluR3 and NMDAR1 and (2) negatively correlated with CA1 and subiculum GluR1 and GluR2 hybridization densities (Table I; Fig. 7).

In the pilocarpine status model, these results indicate that hippocampal AMPA and NMDA receptor subunit mRNA levels dynamically change as rats progressed from the latent to chronic limbic seizure phases, and subunit alterations often correlate with aberrant mossy fiber sprouting. Assuming that AMPA and NMDA subunit mRNA levels are comparable to transcribed proteins, our findings are consistent with the notion that mossy fiber sprouting and spontaneous limbic seizures may affect postsynaptic hippocampal AMPA and NMDA receptor stoichiometry at different poststatus phases. In other words, the mRNA changes are probably maladaptive rather than adaptive and may result in abnormal synaptic functions and neuronal hyperexcitability.

While our findings support the hypothesis that aberrant axon sprouting may affect the subunit composition of glutamate receptors, it is important to emphasize that our experimental design does not preclude other explanations. For example, previous studies of the intrahippocampal kainate and self-sustaining limbic status epilepticus (SSLSE) rat models indicate that aberrant mossy fiber sprouting positively correlates with the in vivo frequency of hippocampal interictal epileptiform discharges and the number of spontaneous limbic seizures (Leite et al., 1996; Mathern et al., 1997a). The

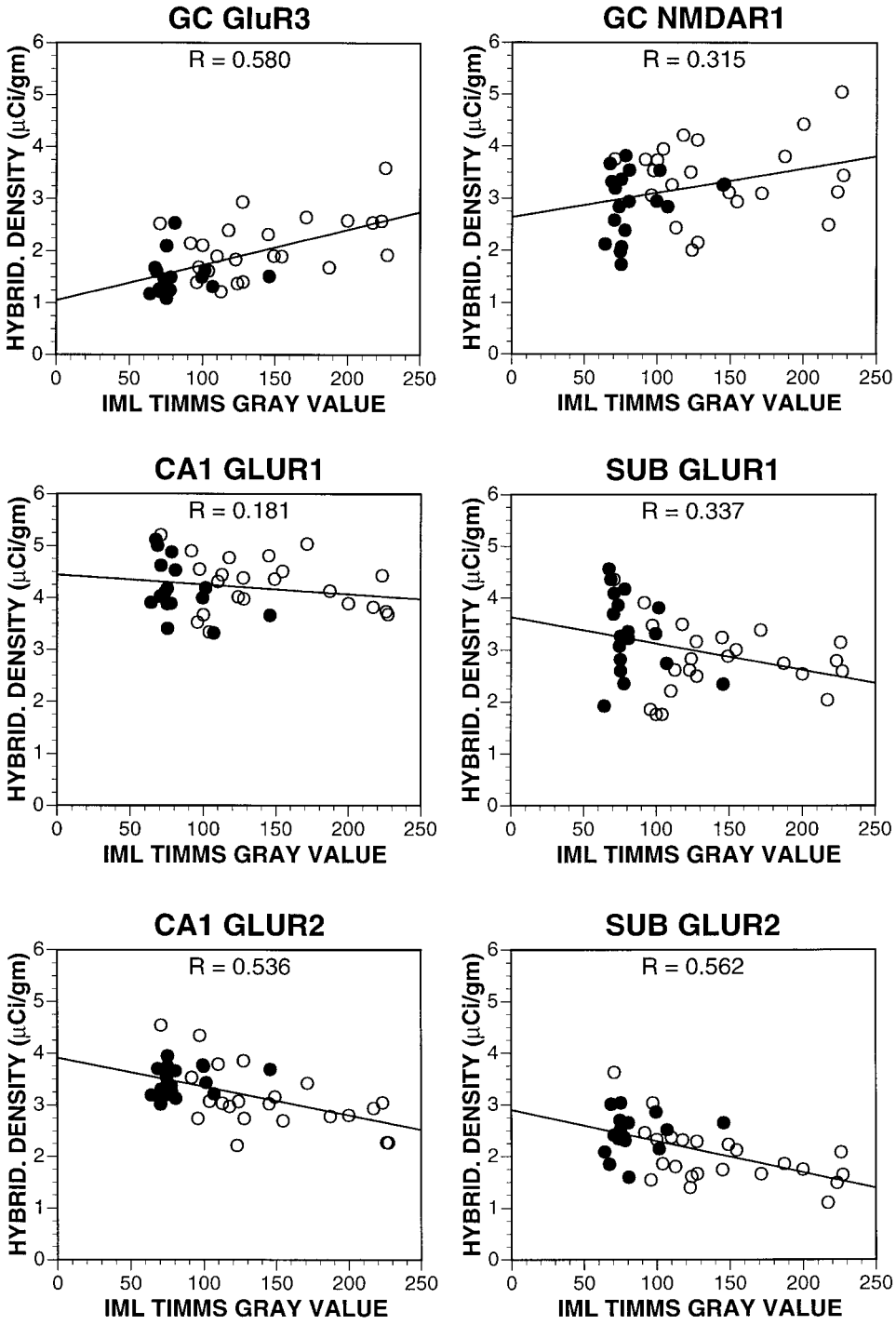

Fig. 7. Linear correlations comparing IML neo-Timm's GVs and AMPA and NMDA hybridization densities. Filled circles indicate control animals and open circles pilocarpine status rats. R-values are indicated above each plot, and *P*-values are shown in Table I (bottom row).

interictal abnormalities begin during the latent phase prior to the onset of the chronic seizures (Mathern et al., 1993). It is therefore possible that our correlations between supragranular neo-Timm's GVs and AMPA and NMDA receptor subunit mRNA levels could be the consequence of increased interictal discharges. In other words, the alterations in glutamate receptor subunits could be from increased synaptic activity secondary to

interictal spikes and/or seizures, but the sprouting itself may not be directly responsible for the subunit alterations. Likewise, the correlations between mossy fiber sprouting and decreased CA1 and subiculum GluR1 and GluR2 mRNA levels could represent regio superior synaptic reorganization. Several rodent anatomic and electrophysiologic studies support the notion that following status epilepticus, aberrant axon sprouting probably occurs around CA1 pyramids (Nadler et al., 1980; Christian and Dudek, 1988; Dudek et al., 1994; Meier and Dudek, 1996; Perez et al., 1996). Our neo-Timm's GV measurements could be an indirect measure of overall hippocampal reactive synaptogenesis after status, and the correlations with CA1 and subiculum AMPA mRNA levels may be from pyramidal neosynaptogenesis and not mossy fiber sprouting. Hence, our data should be interpreted with the understanding that interictal spike activity and/or local reactive synaptogenesis may be other possible explanations for our correlations between AMPA and NMDA mRNA levels and mossy fiber sprouting. This does not distract from our principle conclusion, however, that in the epileptic hippocampus, changes in axon circuitry and neuronal hyperexcitability are likely to be important factors contributing to glutamate receptor subunit changes associated with spontaneous limbic seizures.

Comparison With Prior Animal and Human Studies

In the rodent hippocampus, previous studies indicate that stimuli ranging from minor stress to near-lethal seizures are associated with acute and generally time-limited alterations in AMPA and NMDA receptor subunit mRNA levels, and the response varies depending on the stimulation, subfield, and subunit. For example, several reports have characterized changes in rat hippocampal AMPA and NMDA hybridization densities within hours to a few days following injury or seizures induced from kainate, pilocarpine, limbic kindling, electrolytic lesions, electroshock, intracerebral needle insertion, and stressful handling (Gall et al., 1990; Kamphuis et al., 1992, 1994, 1995; Pollard et al., 1993; Pratt et al., 1993; Wong et al., 1993; Condorelli et al., 1994; Friedman et al., 1994, 1997; Kraus et al., 1994; Lee et al., 1994; Bartanusz et al., 1995; Prince et al., 1995; Gold et al., 1996; Naylor et al., 1996; Lason et al., 1997). These stimuli result in mild agitation or injury without seizures (handling and needle insertion), a few limbic seizures over several hours (electrolytic and electroshock), multiple reactive seizures spaced over days to weeks (kindling), or near-lethal status epilepticus (kainate and pilocarpine). AMPA and NMDA subunit mRNA levels show increased, decreased, or no changes that vary by the method of stimulation and hippocampal subfield. After acute pilocarpine status, rats show decreased hippocampal GluR1 mRNA levels in all subfields by 24 hours poststatus, no change in GluR2 densities, increased granule cell GluR3 levels by 24 hours, and decreased NMDAR1 densities in most subfields for the first 1–3 days (Condorelli et al., 1994; Lason et al., 1997). The acute alterations vary between 50% to 100% of control levels, and nearly all the acute pilocarpine status-related mRNA changes return to baseline within days. Our results show that following pilocarpine status, there were long-term changes in AMPA and NMDA mRNA levels that did not follow the pattern observed immediately after status epilepticus, and these alterations were generally less than 40% of control values (Fig. 6).

This rat study may help to explain recent human neuropathologic findings. For example, in temporal lobe epilepsy patients, we recently showed that most glutamate receptor subunit mRNA and protein levels were increased in epileptic hippocampi compared with nonseizure autopsies (Mathern et al., 1996, 1997b, 1998b,d). In other words, most of the human subunit changes were related to the presence of chronic limbic seizures, while others, such as NMDAR2 immunoreactivity and KA-receptor mRNA levels, were associated or correlated with supragranular mossy fiber sprouting. This would be consistent with our rat pilocarpine status data in that rats with limbic epilepsy show changes in ionotropic receptor subunits that may be associated with both chronic seizures and/or mossy fiber sprouting.

Comparison With Electrophysiologic Studies

Electrophysiologic studies of poststatus or kindled rats show hippocampal neuronal hyperexcitability that is likely the result of alterations in glutamatergic and GABAergic neurotransmission. Our glutamate receptor subunit data complement these findings. For example, following status epilepticus or limbic kindling, in vitro slice and in vivo hippocampal recordings show acute and chronic loss of inhibitory postsynaptic potentials (IPSP) that are likely the result of decreased short-latency GABA-A-mediated inhibition (Franck and Schwartzkroin, 1985; Ashwood et al., 1986; Kapur et al., 1989; Sloviter, 1992; Meier et al., 1992; Williams et al., 1993; Kapur and Coulter, 1995; Mangan et al., 1995; Mangan and Bertram, 1997). It is hypothesized that the acute loss of GABA-A-mediated inhibition is from transient local disconnection of excitatory axons from preserved inhibitory interneurons (Franck et al., 1988; Nakajima et al., 1991; Schwarzer et al., 1997). By the time spontaneous limbic seizures begin, the IPSPs partially or completely recover, and this may represent excitatory fiber reactive synaptogenesis onto interneurons, GABAergic axon sprouting onto deafferented glutamatergic neurons, changes in GABA-A postsynaptic receptor subunit stoichiometry, and/or reductions in GABA transporters (Franck et al., 1988; Davenport et al., 1990; Sloviter, 1992;

Mathern et al., 1995a, 1997a; Williamson et al., 1995; Buckmaster and Dudek, 1997a,b; Kotti et al., 1997; Rempe et al., 1997). There are similar time-dependent changes in excitatory postsynaptic potentials (EPSP) in the same animal models. Following status epilepticus and/or kindling, fascia dentata granule cells, CA1 pyramids, and cells within the entorhinal cortex and basolateral amygdala show epileptiform activity that is locally generated, enhanced after GABAergic blockade, and partly or completely blocked by NMDA and AMPA receptor pharmacologic antagonists (Tauck and Nadler, 1985; Ashwood and Wheal, 1986, 1987; Mody and Heinemann, 1987; Turner and Wheal, 1991; Cronin et al., 1992; Meier et al., 1992; Köhr et al., 1993; Bernard and Wheal, 1995; Bear et al., 1996; Smith and Dudek, 1997; Patrylo and Dudek, 1998). Similar electrophysiologic findings, especially involving NMDA receptors, have been found in human granule cells of hippocampal sclerosis patients with intractable limbic epilepsy (Masukawa et al., 1989, 1992; Urban et al., 1990; Isokawa and Levesque, 1991; Franck et al., 1995).

Our anatomic data is consistent with the idea that changes in EPSPs may in part be explained by alterations in glutamate receptor subunit numbers and/or receptor subunit stoichiometry, and the particular receptor changes may depend on the time after status the animals were studied and the concurrent amount of aberrant axon sprouting (Burnashev et al., 1992; Monyer et al., 1992; Mathern et al., 1997a). For example, we found increased NMDA subunit mRNA levels during the latent phase prior to the onset of spontaneous limbic seizures and significant mossy fiber sprouting. This is consistent with electrophysiologic studies showing enhanced NMDA responsiveness within a few days after seizures and may reflect subacute reactive changes in glutamate receptors unrelated to mossy fiber sprouting (Ashwood and Wheal, 1986, 1987; Mody and Heinemann, 1987; Bernard and Wheal, 1995). Likewise, we found long-term alterations in AMPA and NMDA receptor subunits during the chronic limbic epilepsy phase that correlated with mossy fiber sprouting. This would be consistent with studies showing AMPA- and NMDA-mediated granule cell hyperexcitability in association with aberrant axon sprouting weeks to months after injury (Cronin et al., 1992; Mathern et al., 1992, 1993; Patrylo and Dudek, 1998). However, it should be noted that our pathophysiologic understanding of the limbic epileptogenic process is far from complete. The complex time-dependent and pathophysiologic relationships between axon sprouting, GABA-mediated inhibition, and glutamate-mediated excitation need to be considered concurrently as animals evolve from the latent into the chronic seizure phase (Stelzer et al., 1987). Hence, additional experimental and human studies are necessary to better define the pathophysiology of limbic seizures, but our study supports the concept that postsynaptic glutamate receptors are prominently involved and are linked to aberrant axon sprouting.

Conclusions

In pilocarpine status rats, this study found alterations in hippocampal AMPA and NMDA receptor subunit hybridization densities that changed between the subacute latent to the chronic limbic epilepsy phases and that some subfield GluR1–3 and NMDAR1 alterations correlated with aberrant fascia dentata mossy fiber sprouting. These findings extend previous investigations examining glutamate receptor subunit expression for several hours to days following acute pilocarpine-induced status epilepticus. Furthermore, our results are consistent with electrophysiologic studies showing increased hippocampal glutamatergic neurotransmission at various stages after status epilepticus. We conclude that many acute and chronic electrophysiologic signs of neuronal hyperexcitability may be partially the consequence of changes in glutamate receptor subunit stoichiometry. Finally, the results of this animal study are helpful in interpreting recent human studies in temporal lobe epilepsy patients showing increased hippocampal glutamate receptor subunit mRNA and protein expression associated with limbic seizures and mossy fiber sprouting.

ACKNOWLEDGMENTS

Maria Melendez kindly assisted in manuscript preparation. Special thanks to The Salk Institute and Dr. Jim Boulter in providing the plasmid cDNAs and technical advice.

REFERENCES

Ashwood TJ, Wheal HV. 1986. Extracellular studies on the role of N-methyl-D-aspartate receptors in epileptiform activity recorded from the kainic acid-lesioned hippocampus. Neurosci Lett 67:147–152.

Ashwood TJ, Wheal HV. 1987. The expression of N-methyl-D-aspartate-receptor-mediated component during epileptiform synaptic activity in the hippocampus. Br J Pharmac 91:815–822.

Ashwood TJ, Lancaster B, Wheal HV. 1986. Intracellular electrophysiology of CA1 pyramidal neurones in slices of the kainic acid lesioned hippocampus of the rat. Exp Brain Res 62:189–198.

Babb TL, Lieb JP, Brown WJ, Pretorius J, Crandall PH. 1984a. Distribution of pyramidal cell density and hyperexcitability in the epileptic human hippocampus. Epilepsia 25:721–728.

Babb TL, Brown WJ, Pretorius J, Davenport C, Lieb JP, Crandall PH. 1984b. Temporal lobe volumetric cell densities in temporal lobe epilepsy. Epilepsia 25:729–740.

Babb TL, Kupfer WR, Pretorius JK, Crandall PH, Lévesque MF. 1991. Synaptic reorganization by mossy fibers in human epileptic fascia dentata. Neuroscience 42:351–363.

Bartanusz V, Aubry J-M, Pagliusi S, Jezova D, Baffi J, Kiss JZ. 1995. Stress-induced changes in messenger RNA levels of N-methyl-D-aspartate and AMPA receptor subunits in selected regions of the rat hippocampus and hypothalamus. Neuroscience 66:247–252.

Bear J, Fountain NB, Lothman EW. 1996. Responses of the superficial entorhinal cortex in vitro in slices from naive and chronically epileptic rats. J Neurophysiol 76:2928–2940.

Bernard CL, Wheal HV. 1995. Plasticity of AMPA and NMDA receptor-mediated epileptiform activity in a chronic model of temporal lobe epilepsy. Epilepsy Res 21:95–107.

Bertram EH, Cornett JF. 1993. The ontogeny of seizures in a rat model of limbic epilepsy: Evidence for a kindling process in the development of chronic spontaneous seizures. Brain Res 625: 295–300.

Bertram EH, Cornett JF. 1994. The evolution of a rat model of chronic spontaneous limbic seizures. Brain Res 661:157–162.

Bertram EH, Lothman EW. 1993. Morphometric effects of intermittent kindled seizures and limbic status epilepticus in the dentate gyrus of the rat. Brain Res 603:25–31.

Bertram EH, Lothman EW, Lenn NJ. 1990. The hippocampus in experimental chronic epilepsy: A morphometric analysis. Ann. Neurol 27:43–48.

Boulter J, Hollmann M, O'Shea-Greenfield A, Hartley M, Deneris E, Maron C, Heinemann S. 1990. Molecular cloning and functional expression of glutamate receptor subunit genes. Science 249:1033–1037.

Buckmaster PS, Dudek FE. 1997a. Network properties of the dentate gyrus in epileptic rats with hilar neuron loss and granule cell axon reorganization. J Neurophysiol 77:2685–2696.

Buckmaster PS, Dudek FE. 1997b. Neuron loss, granule cell axon reorganization, and functional changes in the dentate gyrus of epileptic kainate-treated rats. J Comp Neurol 385:385–404.

Burnashev N, Khodorova A, Jonas P, Helm PJ, Wisden W, Monyer H, Seeburg PH, Sakmann B. 1992. Calcium-permeable AMPA-kainate receptors in fusiform cerebellar glial cells. Science 256:1566–1570.

Cavalheiro EA, Leite JP, Bortolotto ZA, Turski WA, Ikonomidou C, Turski L. 1991. Long-term effects of pilocarpine in rats: Structural damage of the brain triggers kindling and spontaneous recurrent seizures. Epilepsia 32:778–782.

Christian EP, Dudek FE. 1988. Characteristics of local excitatory circuits studied with glutamate microapplication in the CA3 area of rat hippocampal slices. J Neurophysiol 59:90–109.

Condorelli DF, Belluardo N, Mudò G, Dell'Albani P, Jiang X, Giuffrida-Stella AM. 1994. Changes in gene expression of AMPA-selective glutamate receptor subunits induced by status epilepticus in rat brain. Neurochem Int 25:367–376.

Cronin J, Dudek FE. 1988. Chronic seizures and collateral sprouting of dentate mossy fibers after kainic acid treatment in rats. Brain Res 474:181–184.

Cronin J, Obenaus A, Houser CR, Dudek FE. 1992. Electrophysiology of dentate granule cells after kainate-induced synaptic reorganization of the mossy fibers. Brain Res 573:305–310.

Davenport CJ, Brown WJ, Babb TL. 1990. Sprouting of GABAergic and mossy fiber axons in dentate gyrus following intrahippocampal kainate in the rat. Exp Neurol 109:180–190.

de Lanerolle NC, Kim JH, Robbins RJ, Spencer DD. 1989. Hippocampal interneuron loss and plasticity in human temporal lobe epilepsy. Brain Res 495:387–395.

Dudek FE, Spitz M. 1997. Hypothetical mechanisms for the cellular and neurophysiologic basis of secondary epileptogenesis: Proposed role of synaptic reorganization. J Clin Neurophysiol 14:90–101.

Dudek FE, Obenaus A, Schweitzer JS, Wuarin J.-P. 1994. Functional significance of hippocampal plasticity in epileptic brain: Electrophysiological changes of the dentate granule cells associated with mossy fiber sprouting. Hippocampus 4:259–265.

Franck JE, Schwartzkroin PA. 1985. Do kainate-lesioned hippocampi become epileptogenic? Brain Res 329:309–313.

Franck JE, Kunkel DD, Baskin DG, Schwartzkroin PA. 1988. Inhibition in kainate-lesioned hyperexcitable hippocampi: Physiologic, autoradiographic, and immunocytochemical observations. J Neurosci 8:1991–2002.

Franck JE, Pokorny J, Kunkel DD, Schwartzkroin PA. 1995. Physiologic and morphologic characteristics of granule cell circuitry in human epileptic hippocampus. Epilepsia 36:543–558.

Friedman LK, Pellegrini-Giampietro DE, Sperber EF, Bennett MVL, Moshé SL, Zukin RS. 1994. Kainate-induced status epilepticus alters glutamate and $GABA_A$ receptor gene expression in adult rat hippocampus: An *in situ* hybridization study. J Neurosci 14:2697–2707.

Friedman LK, Sperber EF, Moshé SL, Bennett MV, Zukin RS. 1997. Developmental regulation of glutamate and $GABA_A$ receptor gene expression in rat hippocampus following kainate-induced status epilepticus. Dev Neurosci 19:529–542.

Gall C, Isackson PJ. 1989. Limbic seizures increase neuronal production of messenger RNA for nerve-growth factor. Science 245:758–761.

Gall C, Sumikawa K, Lynch G. 1990. Levels of mRNA for a putative kainate receptor are affected by seizures. Proc Natn Acad Sci USA 87:7643–7647.

Gold SJ, Hennegriff M, Lynch G, Gall CM. 1996. Relative concentrations and seizure-induced changes in mRNAs encoding three AMPA receptor subunits in hippocampus and cortex. J Comp Neurol 365:541–555.

Houser CR, Miyashiro JE, Swartz BE, Walsh GO, Rich JR, Delgado-Escueta AV. 1990. Altered patterns of dynorphin immunoreactivity suggest mossy fiber reorganization in human hippocampal epilepsy. J Neurosci 10:267–282.

Isokawa M, Lévesque MF. 1991. Increased NMDA responses and dendritic degeneration in human epileptic hippocampal neurons in slices. Neurosci Lett 132:212–216.

Kamphuis W, Monyer H, De Rijk TC, Lopes da Silva FH. 1992. Hippocampal kindling increases the expression of glutamate receptor-A Flip and -B Flip mRNA in dentate granule cells. Neurosci Lett 148:51–54.

Kamphuis W, De Rijk TC, Talamini LM, Lopes da Silva FH. 1994. Rat hippocampal kindling induces changes in the glutamate receptor mRNA expression patterns in dentate granule neurons. Eur J Neurosci 6:1119–1127.

Kamphuis W, Hendriksen H, Diegenbach PC, Lopes da Silva FH. 1995. N-methyl-D-aspartate and kainate receptor gene expression in hippocampal pyramidal and granular neurons in the kindling model of epileptogenesis. Neuroscience 67:551–559.

Kapur J, Coulter DA. 1995. Experimental status epilepticus alters γ-aminobutyric acid type A receptor function in CA1 pyramidal neurons. Ann Neurol 38:893–900.

Kapur J, Stringer JL, Lothman EW. 1989. Evidence that repetitive seizures in the hippocampus cause a lasting reduction of GABAergic inhibition. J Neurophysiol 61:417–426.

Köhr G, De Koninck Y, Mody I. 1993. Properties of NMDA receptor channels in neurons acutely isolated from epileptic (kindled) rats. J Neurosci 13:3612–3627.

Kornblum HI, Chugani HT, Tatsukawa K, Gall CM. 1994. Cerebral hemidecortication alters expression of transforming growth factor alpha mRNA in the neostriatum of developing rats. Mol Brain Res 21:107–114.

Kotti T, Riekkinen PJ, Miettinen R. 1997. Characterization of target cells for aberrant mossy fiber collaterals in the dentate gyrus of epileptic rat. Exp Neurol 146:323–330.

Kraus JE, Yeh G-C, Bonhaus DW, Nadler JV, McNamara JO. 1994. Kindling induces the long-lasting expression of a novel population of NMDA receptors in hippocampal region CA3. J Neurosci 14:4196–4205.

Lason W, Turchan J, Przewlocki R, Machelska H, Labuz D, Przewlocka B. 1997. Effects of pilocarpine and kainate-induced seizures on N-methyl-D-aspartate receptor gene expression in the rat hippocampus. Neuroscience 78:997–1004.

Lee S, Miskovsky J, Williamson J, Howells R, Devinsky O, Lothman E, Christakos S. 1994. Changes in glutamate receptor and proenkephalin gene expression after kindled seizures. Mol Brain Res 24:34–42.

Leite JP, Bortolotto ZA, Cavalheiro EA. 1990. Spontaneous recurrent seizures in rats: An experimental model of partial epilepsy. Neurosci Biobehav Rev 14:511–517.

Leite JP, Babb TL, Pretorius JK, Kuhlman PA, Yeoman KM, Mathern GW. 1996. Neuron loss, mossy fiber sprouting, and interictal spikes after intrahippocampal kainic acid in developing rats. Epilepsy Res 26:219–231.

Lemos T, Cavalheiro EA. 1995. Suppression of pilocarpine-induced status epileticus and the late development of epilepsy in rats. Exp Brain Res 102:423–428.

Longo BM, Mello LEAM. 1997. Blockade of pilocarpine- or kainate-induced mossy fiber sprouting by cycloheximide does not prevent subsequent epileptogenesis in rats. Neurosci Lett 226: 163–166.

Lorente de Nó R. 1934. Studies on the structure of the cerebral cortex. II. Continuation of the study of the ammonic system. J Psychol Neurol 45:113–177.

Mangan PS, Bertram EH. 1997. Shortened-duration $GABA_A$ receptor-mediated synaptic potentials underlie enhanced CA1 excitability in a chronic model of temporal lobe epilepsy. Neuroscience 80:1101–1111.

Mangan PS, Rempe DA, Lothman EW. 1995. Changes in inhibitory neurotransmission in the CA1 region and dentate gyrus in a chronic model of temporal lobe epilepsy. J Neurophysiol 74:829–840.

Masukawa LM, Higashima M, Kim JH, Spencer DD. 1989. Epileptiform discharges evoked in hippocampal brain slices from epileptic patients. Brain Res 493:168–174.

Masukawa LM, Uruno K, Sperling M, O'Connor MJ, Burdette LJ. 1992. The functional relationship between antidromically evoked field responses of the dentate gyrus and mossy fiber reorganization in temporal lobe epileptic patients. Brain Res 579:119–127.

Mathern GW. 1998a. Hippocampal pathophysiology in experimental models. In Kotagal P, Lüders H, editors. The epilepsies: Etiologies and prevention. New York: Academic Press (in press).

Mathern GW. 1998b. Reactive synaptogenesis as a consequence of status epilepticus. In Treiman DM, Wasterlain CG, editors. Status epilepticus: Mechanisms and management. New York: Lippincott-Raven Publisher (in press).

Mathern GW, Kupfer WR, Pretorius JK, Babb TL, Lévesque MF. 1992. Onset and patterns of hippocampal spouting in the rat kainate seizure model: Evidence for progressive cell loss and neoinnervation in regio inferior and superior. Dendron 1:69–84.

Mathern GW, Cifuentes F, Leite JP, Pretorius JK, Babb TL. 1993. Hippocampal EEG excitability and chronic spontaneous seizures are associated with aberrant synaptic reorganization in the rat intrahippocampal kainate model. Electroencephalogr Clin Neurophysiol 87:326–339.

Mathern GW, Babb TL, Pretorius JK, Leite JP. 1995a. Reactive synaptogenesis and neuron densities for neuropeptide Y, somatostatin, and glutamate decarboxylase-immunoreactivity in the epileptogenic human fascia dentata. J Neurosci 15:3990–1404.

Mathern GW, Babb TL, Vickrey BG, Melendez M, Pretorius JK. 1995b. The clinical-pathogenic mechanisms of hippocampal neuron loss and surgical outcomes in temporal lobe epilepsy. Brain 118:105–118.

Mathern GW, Pretorius JK, Babb TL. 1995c. Quantified patterns of mossy fiber sprouting and neuron densities in hippocampal and lesional seizures. J Neurosurg 82:211–219.

Mathern GW, Leite JP, Babb TL, Pretorius JK, Kuhlman PA, Mendoza D, Fried I, Sakamoto AC, Assirati JA, Adelson PD, Peacock WJ. 1996. Aberrant hippocampal mossy fiber sprouting correlates with greater NMDAR2 receptor staining. NeuroReport 7:1029–1035.

Mathern GW, Bertram EH, Babb TL, Pretorius JK, Kuhlman PA, Spradlin S, Mendoza D. 1997a. In contrast to kindled seizures, the frequency of spontaneous epilepsy in the limbic status model correlates with greater aberrant fascia dentata excitatory and inhibitory axon sprouting, and increased staining for NMDA, AMPA, and GABA-A receptors. Neuroscience 77:1003–1019.

Mathern GW, Pretorius JK, Kornblum HI, Mendoza D, Lozada A, Leite JP, Chimelli LMC, Fried I, Sakamoto AC, Assirati JA, Lévesque MF, Adelson PD, Peacock WJ. 1997b. Human hippocampal AMPA and NMDA mRNA levels in temporal lobe epilepsy patients. Brain 120:1937–1959.

Mathern GW, Babb TL, Armstrong DL. 1997c. Hippocampal sclerosis. In Engel J, Pedley TA, editors. Epilepsy: A comprehensive textbook. New York: Raven Press. p 133–155.

Mathern GW, Price G, Rosales C, Pretorius JK, Lozada A, Mendoza D. 1998a. Anoxia during kainate status epilepticus shortens behavioral convulsions but generates hippocampal neuron loss and supragranular mossy fiber sprouting. Epilepsy Res 30:133–151.

Mathern GW, Pretorius JK, Mendoza D, Lozada A, Leite JP, Chimelli LMC, Fried I, Peacock WJ, Sakamoto AC, Assirati JA, Lévesque MF, Adelson PD. 1998b. Increased hippocampal AMPA and NMDA receptor subunit immunoreactivity in temporal lobe epilepsy patients. J Neuropath Exp Neurol 57:615–634.

Mathern GW, Pretorius JK, Kornblum HI, Mendoza D, Lozada A. 1998c. AMPA and NMDA mRNA levels in the pilocarpine model of spontaneous limbic epilepsy. Soc Neurosci Abstr 24:1207.

Mathern GW, Pretorius JK, Kornblum HI, Mendoza D, Lozada A, Leite JP, Chimelli L, Born DE, Fried I, Sakamoto AC, Assirati JA, Peacock WJ, Ojemann GA, Adelson PD. 1998d. Altered hippocampal kainate-receptor mRNA levels in temporal lobe epilepsy patients. Neurobiol Disease (in press).

McNamara JO. 1994. Cellular and molecular basis of epilepsy. J Neurosci 14:3413–3425.

Meier CL, Dudek FE. 1996. Spontaneous and stimulation-induced synchronized burst afterdischarges in the isolated CA1 of kainate-treated rats. J Neurophysiol 76:2231–2239.

Meier CL, Obenaus A, Dudek FE. 1992. Persistent hyperexcitability in isolated hippocampal CA1 of kainate-lesioned rats. J Neurophysiol 68:2120–2127.

Mody I, Heinemann U. 1987. NMDA receptors of dentate gyrus granule cells participate in synaptic transmission following kindling. Nature 326:701–704.

Monyer H, Sprengel R, Schoepfer R, Herb A, Higuchi M, Lomeli H, Burnashev N, Sakmann B, Seeburg PH. 1992. Heteromeric NMDA receptors: molecular and functional distinction of subtypes. Science 256:1217–1221.

Nadler JV, Perry BW, Gentry C, Cotman CW. 1980. Loss and reacquisition of hippocampal synapses after selective destruction of CA3–CA4 afferents with kainic acid. Brain Res 191:387–403.

Nakajima S, Franck JE, Bilkey D, Schwartzkroin PA. 1991. Local circuit synaptic interactions between CA1 pyramidal cells and interneurons in the kainate-lesioned hyperexcitable hippocampus. Hippocampus 1:67–78.

Naylor P, Stewart CA, Wright SR, Pearson RCA, Reid IC. 1996. Repeated ECS induces GluR1 mRNA but not NMDAR1A-G mRNA in the rat hippocampus. Mol Brain Res 35:349–353.

Okazaki MM, Evenson DA, Nadler JV. 1995. Hippocampal mossy fiber sprouting and synapse formation after status epilepticus in rats: Visualization after retrograde transport of biocytin. J Comp Neurol 352:515–534.

Patrylo PR, Dudek FE. 1998. Physiological unmasking of new glutamatergic pathways in the dentate gyrus of hippocampal slices from kainate-induced epileptic rats. J Neurophysiol 79:418–429.

Perez Y, Morin F, Beaulieu C, Lacaille J-C. 1996. Axonal sprouting of CA1 pyramidal cells in hyperexcitable hippocampal slices of kainate-treated rats. Eur J Neurosci 8:736–748.

Pollard H, Héron A, Moreau J, Ben-Ari Y, Khrestchatisky M. 1993. Alterations of the GluR-B AMPA receptor subunit flip/flop expression in kainate-induced epilepsy and ischemia. Neuroscience 57:545–554.

Pratt GD, Kokaia M, Bengzon J, Kokaia Z, Fritschy J.-M., Möhler H, Lindvall O. 1993. Differential regulation of N-methyl-D-aspartate receptor subunit messenger RNAs in kindling-induced epileptogenesis. Neuroscience 57:307–318.

Prince HK, Conn PJ, Blackstone CD, Huganir RL, Levey AI. 1995. Down-regulation of AMPA receptor subunit GluR2 in amygdaloid kindling. J Neurochem 64:462–465.

Rempe DA, Bertram EH, Williamson JM, Lothman EW. 1997. Interneurons in area CA1 stratum radiatum and stratum oriens remain functionally connected to excitatory synaptic input in chronically epileptic animals. J Neurophysiol 78:1504–1515.

Schwarzer C, Tsunashima K, Wanzenböck C, Fuchs K, Sieghart W, Sperk G. 1997. $GABA_A$ receptor subunits in the rat hippocampus II: Altered distribution in kainic acid-induced temporal lobe epilepsy. Neuroscience 80:1001–1017.

Sloviter RS. 1992. Possible functional consequences of synaptyic reorganization in the dentate gyrus of kainate-treated rats. Neurosci Lett 137:91–96.

Smith BN, Dudek FE. 1997. Enhanced population responses in the basolateral amygdala of kainate-treated, epileptic rats in vivo. Neurosci Lett 222:1–4.

Stelzer A, Slater NT, ten Bruggencate G. 1987. Activation of NMDA receptors blocks GABAergic inhibition in an *in vitro* model of epilepsy. Nature 326:698–701.

Tauck DL, Nadler JV. 1985. Evidence of functional mossy fiber sprouting in hippocampal formation of kainic acid-treated rats. J Neurosci 5:1016–1022.

Turner DA, Wheal HV. 1991. Excitatory synaptic potentials in kainic acid-denervated rat CA1 pyramidal neurons. J Neurosci 11:2786–2794.

Urban L, Aitken PG, Friedman A, Somjen GG. 1990. An NMDA-mediated component of excitatory synaptic input to dentate granule cells in 'epileptic' hippocampus studied in vitro. Brain Res 515:319–322.

Wieser HG, Engel J Jr, Williamson PD, Babb TL, Gloor P. 1993. Surgically remediable temporal lobe syndromes. In Engel J, Jr, editor. Surgical treatment of the epilepsies, 2nd edition. New York: Raven Press. p 49–63.

Williams SF, Colling SB, Whittington MA, Jefferys JGR. 1993. Epileptic focus induced by intrahippocampal cholera toxin in rat: Time course and properties in vivo and in vitro. Epilepsy Res 16:137–146.

Williamson A, Telfeian AE, Spencer DD. 1995. Prolonged GABA responses in dentate granule cells in slices isolated from patients with temporal lobe sclerosis. J Neurophysiol 74:378–387.

Wong ML, Smith MA, Licinio J, Doi SQ, Weiss SRB, Post RM, Gold PW. 1993. Differential effects of kindled and electrically induced seizures on a glutamate receptor (GluR1) gene expression. Epilepsy Res 14:221–227.

Wuarin J-P, Dudek FE. 1996. Electrographic seizures and new recurrent excitatory circuits in the dentate gyrus of hippocampal slices from kainate-treated epileptic rats. J Neurosci 16:4438–4448.